Flachlamps for Remote Fluorescence Characterization of Oil Slicks

Andersson, P. S; Montan, Sune; Svanberg, Sune

1986

FLASHLAMPS FOR REMOTE FLUORESCENCE CHARACTERIZATION OF OIL SLICKS

P. S. Andersson, S. Montán and S. Svanberg

Lund Institute of Technology

Department of Physics

LUND REPORTS ON ATOMIC PHYSICS

LRAP-57

January 1986

CONTENTS

Page

1. INTRODUCTION.....3

2. FLASHLAMPS.....4

3. LAMP POWER SUPPLIES.....6

4. REFLECTORS.....9

5. LABORATORY TEST.....15

6. FIELD TEST.....19

7. DISCUSSION.....27

8. CONSTRUCTION CONSIDERATIONS.....29

Acknowledgements.....31

References.....32

FLASHLAMPS FOR REMOTE CHARACTERIZATION OF OIL SLICKS

1. INTRODUCTION

Oil has become an increasingly important raw product. It is fundamental to our welfare and a highly industrialized society is dependent on frequent and regular deliveries of oil. However, spills from these transports are a great threat to coastal regions. An efficient surveillance system that makes adequate counter measures possible is therefore desirable. A side-looking airborne radar (SLAR) is a powerful system that is now being used operationally. The SLAR has the great advantage over optical detection systems of being weather-independent. However, it gives little information of the nature of the oil. Such information can be obtained by fluorescence methods. As shown, e.g., in Refs. [1, 2, 3, 4] refined, crude and heavy fuel oils fluoresce differently, the peak wavelength being shorter and the intensity higher for more refined products. Ref. [1] addresses the possibilities to construct a simple and effective laser-induced fluorescence-sensing system for airborne characterization of oil spills as a complement to the SLAR system. Spills would then be detected by SLAR at normal flying altitudes and the fluorosensor would be used for oil characterization in a second slick traverse at low altitude. This concept is outlined in Fig. 1.1. The present report deals with the alternative to use flashlamps

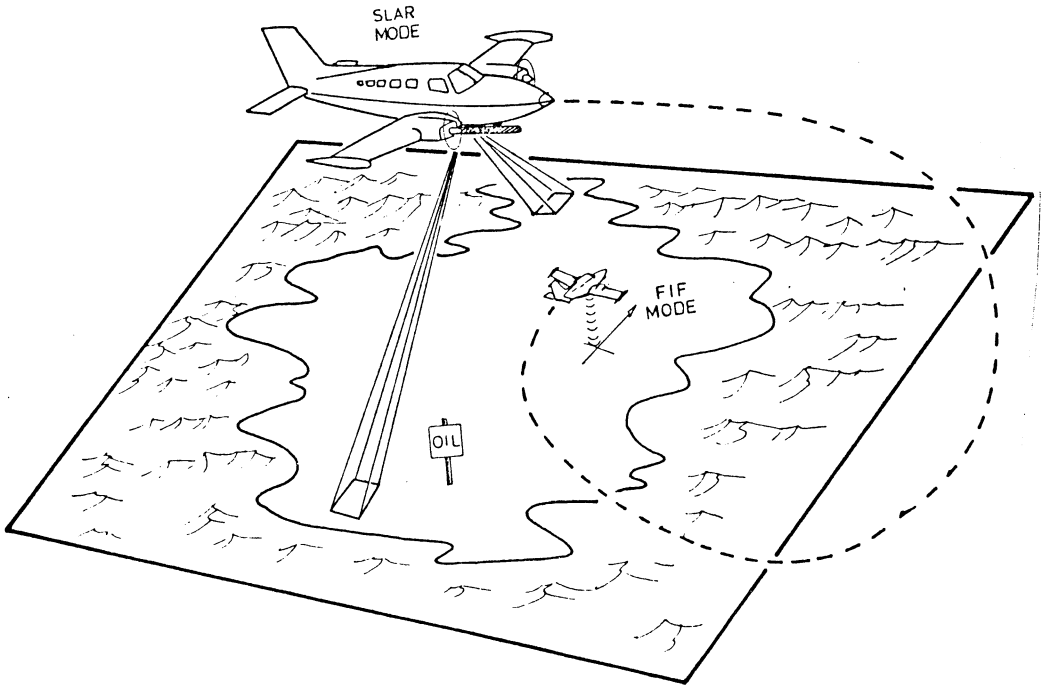

Fig. 1.1: SLAR detection followed by flashlamp-induced fluorescence (FIF) characterization of a marine oil spill.

instead of lasers to induce the fluorescence. Flashlamps are comparatively cheap, have a better conversion efficiency and are able to produce light pulses containing considerably more energy than most lasers (exceptions being made for the most extreme lasers), but they do not have the well-defined beam and monochromaticity of a laser. The flashlamp must be filtered and it has to be directed towards the target by means of a reflector. This report deals with these considerations. In Chapter 2 different properties of flashlamps are summarized. In the subsequent chapters some aspects of the electrical and optical construction of a flashlamp system are considered. In Chapter 5 laboratory measurements foregoing field tests presented in Chapter 6 are described. Finally, conclusions are drawn and important features of an airborne system are discussed.

2. FLASHLAMPS

A flashlamp is a gas discharge light source, in which the light is produced in a plasma. The gas filling is generally one of the noble gases krypton or xenon. The plasma emits radiant energy over a wide range of wavelengths, from far infrared to ultraviolet. The discharge is initiated by causing a spark streamer to form between the electrodes. As this channel grows, the resistance of the lamp drops rapidly. The electrons in the channel equilibrate in a high temperature distribution very quickly and ionize and heat the plasma through collisions. The radiation is made up of line emission from transitions between bound energy states in the atoms and ions of the plasma and continous emission from ion-electron recombinations and Bremsstrahlung radiation from electrons accelerated during collisions with ions. At pressures above 500 millibar and current densities above 3500 A/cm^2 the continous emission is dominant [5].

Xenon is generally chosen as the gas fill in flashlamps, since it yields the highest output efficiency. For short pulse and high current density applications the lower atomic weight noble gases krypton, argon, neon and helium may yield a higher peak brightness. Except for krypton, these gases are not available as a commercial standard, though. Krypton is sometimes used because its line radiation matches the absorption spectra of some solid state materials, including Nd:YAG.

The spectral distribution of the emitted light is primarily a function of two parameters as far as the blackbody radiation (the continous emission) is concerned. These are the lamp current density J, and the internal diameter of the lamp, D. D is also called the bore diameter. The effective blackbody temperature is approximately [6]

$$T=\left[(9450*D^{0.03}*J^{0.01})^6 + (93*D^{0.27}*J^{0.34})^6 \right]^{1/6} \qquad (2.1)$$

When the current pulse in a flashlamp builds up, the atomic line radiation first appears. As the plasma heats, the blackbody emission turns up. When the plasma cools, the blackbody emission is the last to disappear. At short pulses (10 µs or less) the efficiency becomes lower since a large part of the electrical energy goes into heating the lamp wall. A typical lamp spectrum is shown in Fig. 2.1 [7].

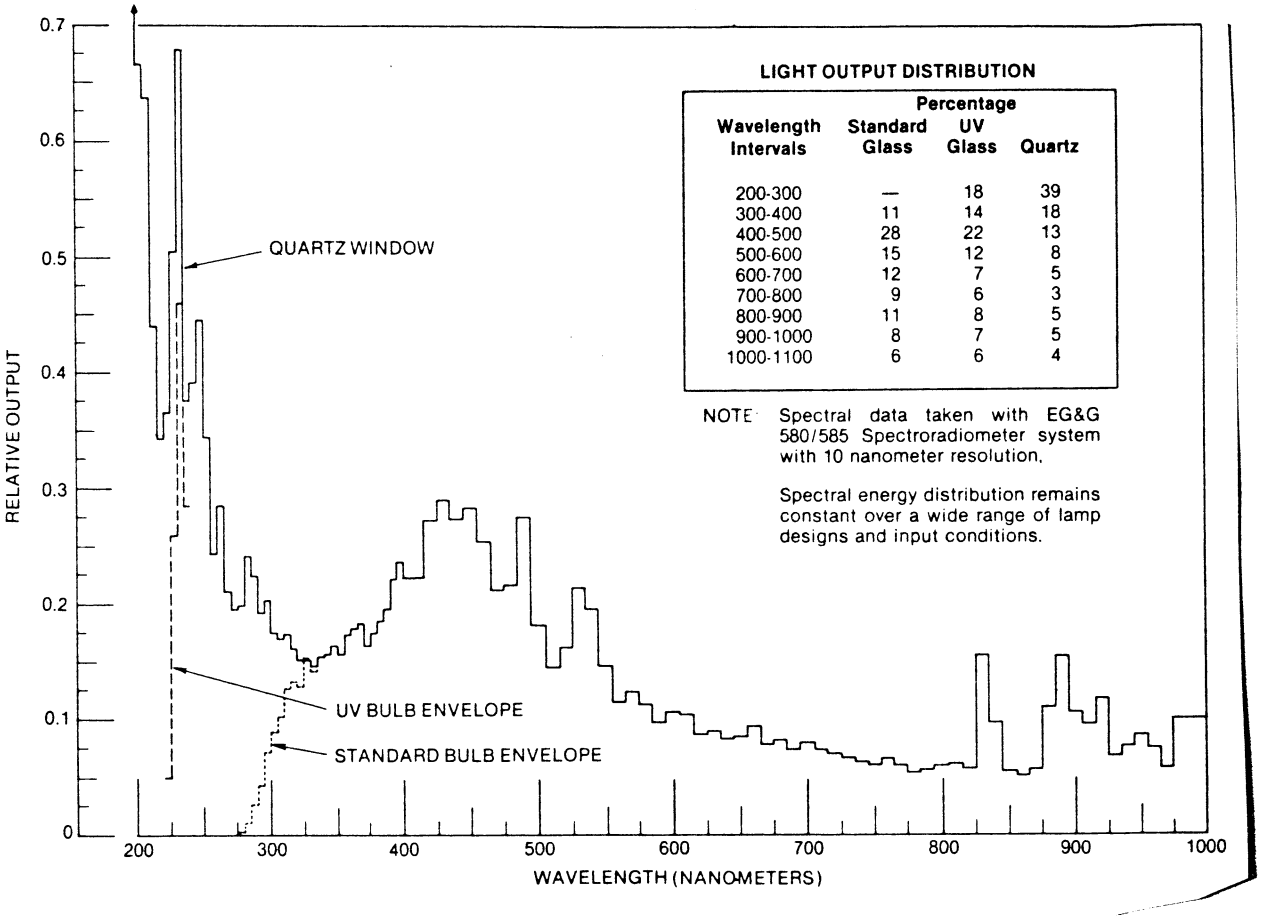

Fig. 2.1: Typical spectrum of a xenon-filled flashlamp (from Ref. [7]).

The material of the flashlamp envelope is usually quartz. Glass does not permit as high energy loads as quartz. The UV transmission of natural fused quartz leads to the production of ozone in those applications where the light reaches air. UV-absorbing fused silica envelopes are available, the most common material being titanium oxide doped natural fused silica, which absorbs light of wavelengths below 240 nm (cf. Fig. 2.1). The maximum allowable energy loading is reduced by about 20 % when UV-absorbing quartz is used. The UV absorption of impurities in the envelope material, which leads to darkening (solarization), will finally decrease the useful light output, also if undoped material is used.

The lifetime of a flashlamp can be estimated from the single shot explosion energy E_x. At input energies exceeding $0.2E_x$ and bore diameters less than 6 mm the lifetime in number of pulses approximately follows the relation

$$\text{Lifetime} = (E/E_x)^{-8.5} \qquad (2.2)$$

There are three processes which limit the lifetime of a flashlamp. These are the solarization mentioned earlier, electrode sputtering and envelope erosion. Electrode sputtering puts the limit when the lamp is operated at low input energies, less than $0.2E_x$. It appears as a dark deposit on the lamp wall and will after some time reduce the light output. Envelope erosion becomes dominant at high peak powers. A small portion of the quartz wall is vaporized by the plasma heat. It condenses in the crystalline state and appears as a white powder. This powder reduces light output and increases wall heating.

A parameter that confines the repetition rate for flashlamps is the recovery time. After a current pulse, the lamp resistance remains low

during this time due to ions with long lifetimes in the plasma. When operated at high repetition rates the charge capacitor must be disconnected from the lamp during this time. The recovery time is of the order of 1 ms and is what primarily prevents flashlamps to be run at repetition rates exceeding 500 Hz [5,6].

The important properties of flashlamps for the purposes studied here are short pulse time (cf. Chapter 3), high pulse power, high intensity per arc length unit, great yield of UV-light, low bore diameter, high peak power, and of course high explosion energy and high average power.

The pulse time must be short (a few µs) since the detection system should be opened as short time as possible to minimize daylight influence. For similar reasons the pulse power must be high so that the signal photons reaching the detection telescope can compete with the daylight photons. The arc length should be small to keep the divergence of the exciting light beam low. However, at short arc lengths, the light output efficiency is low (less than 10 %). Therefore the intensity per arc length unit is a more relevant parameter. The arc length should still be kept small in comparison to the focal length of the reflector (cf. Chapter 4). To achieve a high current density, a low bore diameter is required. A high current density is desired as it enhances the UV output. The explosion energy is relevant for the lifetime and pulse energy of the lamp according to eq. 2.2. The maximum average power, finally, determines the maximum repetition rate (as far it is not limited by the hold-off characteristics) that can be used for a given pulse energy. Table 2.1 shows some examples of commercially available flahlamps and their parameter values.

Manufacturer	Model No.	Pulse width (µs)	Pulse average power (MW)	Arc length (mm)	Explosion energy (J)	Maximum average power (W)
Noblelight	SAPX 10015	20	8	1.5	40	100
EG & G	1PU-1	1-15	2-30	1.0	30	40
EG & G	2PU-3	1-15	4-60	3.0	60	75
EG & G	3PU-4	1-15	7-100	4.0	100	100
Xenon corp.	N-722C	1.5	13	3.0-3.5	20	75
Xenon corp.	N-723C	2.5	40	5.0-7.0	100	100
Xenon corp.	N-787B	0.01	0.05	0.8		

Table 2.1: Some relevant, commercially available, flashlamps for an airborne fluorosensor.

3. LAMP POWER SUPPLIES

The electrical energy discharged in a flashlamp pulse is stored in a capacitor that is recharged after each pulse. The voltage of this storage capacitor is generally chosen to be smaller than the breakdown voltage of the lamp. The spark causing the initial ionization of the gas is instead produced by a trigger circuit. Two different trigger circuits can be used, an external or a series trigger circuit. These

are shown in Figs. 3.1.a and 3.1.b. In the external triggering the ignition is brought about by a high voltage pulse at the external wall of the lamp. The pulse is applied by means of a closely wrapped helix and creates a voltage gradient between the electrodes. This method has the advantages of requiring few components and being cost effective. However, high voltage is exposed and may be hazardous at high altitudes and humid environments.

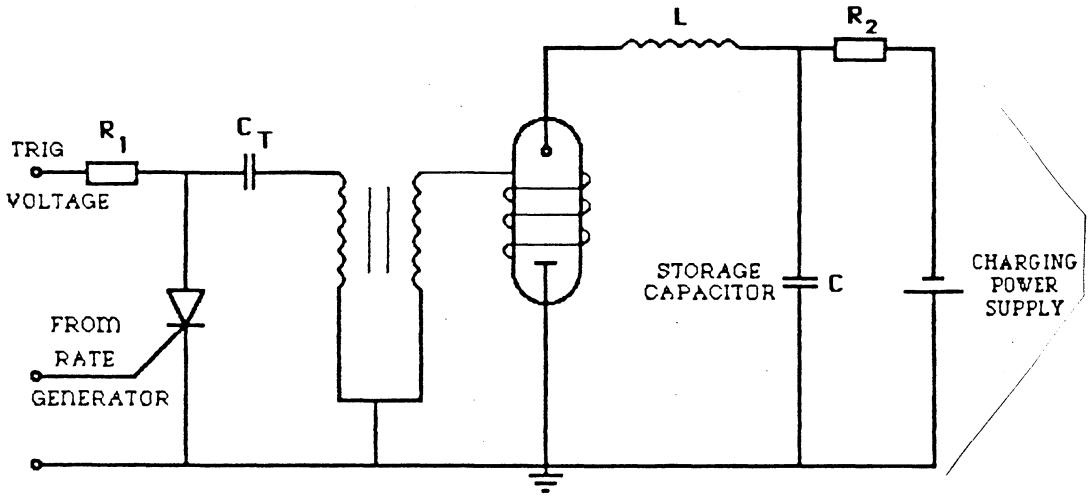

Fig. 3.1.a: External trigger circuit.

The series triggering (Fig. 3.1.b) does not expose any high voltage. Here, the ignition is produced by a high voltage pulse from a trigger transformer in series with the storage capacitor. This method is impossible to use in applications where fast risetime and short pulses are wanted, due to the transformer inductive load.

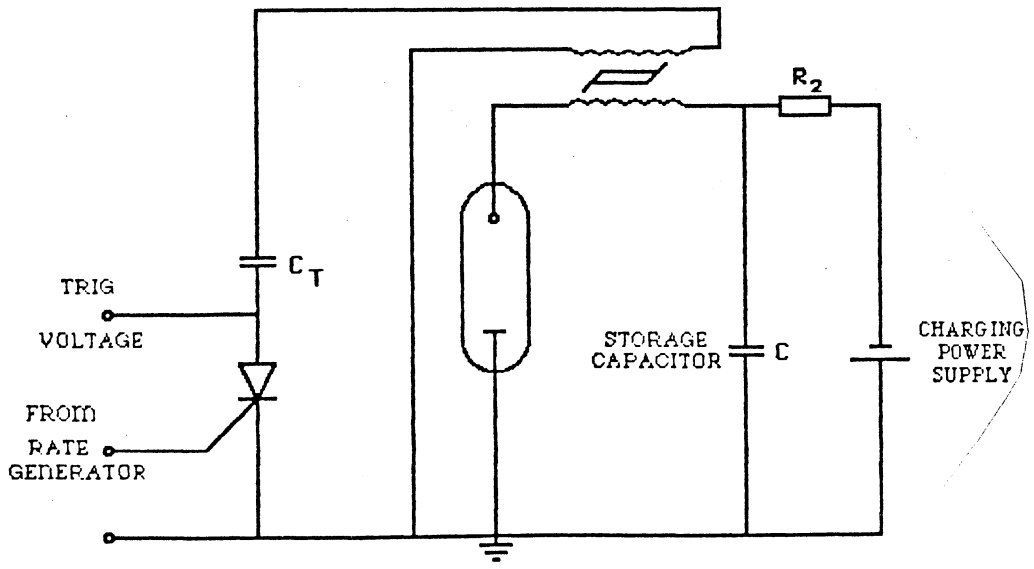

Fig. 3.1.b: Series trigger circuit.

Simmer operation, Fig. 3.2, offers an attractive combination. A low power dc discharge is maintained through the lamp between the pulses. Many advantages are gained by running the lamp in this way, such as: The lamp can be trigged via a simple thyristor, thus allowing short pulses and fast risetimes without any high voltage exposure; the lamp lifetime is increased; the lamp efficiency is improved; it allows a

higher repetition rate; and radio-frequency interferences are reduced. However, as can be seen in the figure, this operation mode requires an additional power supply.

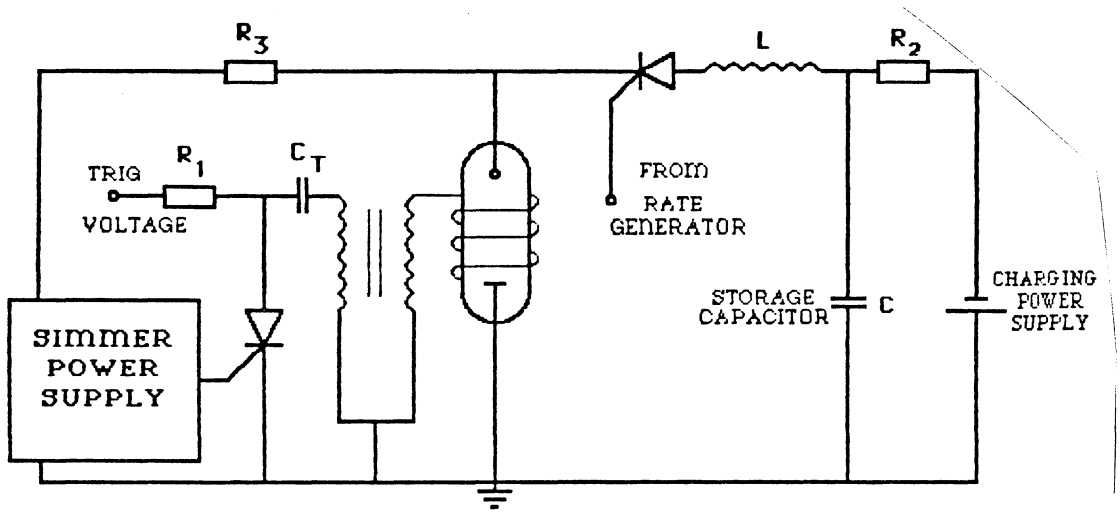

Fig. 3.2: Lamp simmer circuit.

The weight of the lamp power supply is determined by two factors: The maximum electrical energy discharged in each pulse and the maximum average power. The maximum pulse energy decides the storage capacitor size. The stored electrical energy $E=0.5*CU^2$, where C is the storage capacitance and U the voltage over the capacitor. The maximum average power is crucial to the weight of the charging power supply. In Table 3.1 the weights of some charging power supplies and storage capacitors are given. An external trig circuit is also necessary, and a simmer supply may be added. The external trig circuit weighs about 1 kg and a simmer supply (1000 V / 100 mA) approximately 3 kg. For example, for a lamp that should be run in the simmer mode at 10 Hz with a maximum pulse energy of 10 J and a voltage over the storage capacitor of 1000 V, a 100 W (10 J * 10 Hz) charging power supply and a 20 µF (10 J /(0.5 * (1000 V)^2)) storage capacitor are required, giving a total weight of 8 kg (3.1 kg + 0.8 kg + 1 kg + 3 kg) with external trig and simmer circuits included.

Charging power supply		Storage capacitor (max. 1000 V)	
Maximum average power (W)	Weight (kg)	Capacitance (µF)	Weight (kg)
20	1.3	4	0.2
100	3.1	20	0.8
200	5.3	40	1.6
500	12.0	100	4.0
1000	18.0	200	8.0

Table 3.1: Weights of some charging power supplies and storage capacitors.

4. REFLECTORS.

In an active airborne remote sensing system light is emitted as well as detected. Both an intense irradiance at the target and a small detection field-of-view are required for a good signal to background ratio. That means that the light output divergence has to be kept small. A laser source has often this quality while a flashlamp system suffers from a higher divergence.

The lamp radiates uniformly in all directions, hence, in order to collimate the light, some kind of telescope is required. A mirror telescope can, compared to a lens telescope, have a much higher collection efficiency. That means, a mirror can cover a greater solid angle as seen from the lamp than a lens and therefore collect more of the emitted light. A greater part of the lamp power will be directed towards the target causing a higher utilization of the energy. Thus a mirror telescope is preferable. Since the target distance is large, the output beam must be almost parallel. An infinitely small point source in the focal point of a parabolic reflector should thus be the perfect choice for the transmitting system. However, one is limited to a small lamp in front of a reflector, either spherical or parabolic. The spherical shape can substitute the paraboloid for large f-numbers. The contributing mechanisms to the image spread has to be studied when selecting the type of reflector. There are three different kinds of mechanisms: diffraction, aberration and manufacturing tolerances.

A spherical reflector suffers from spherical aberration, especially if a high collection efficiency should be reached. Parabolic reflectors are, on the other hand, more complicated to produce. For a reasonable price a less perfect surface quality may be tolerated. The diffraction is the physically limiting contribution and can not be circumvented. It is dependent only on the telescope aperture. The three mechanisms together with the price and construction considerations have to be weighed in the choice of reflector.

In a simplified example the significance of the spherical aberration can be estimated. Assume a small surface area dS_1 on the lamp , with the normal directed along the optical axis for the mirror, emitting light of power P_1 . Further, assume the reflector to cover the solid angle Ω_1 , seen from the lamp. The power reaching the reflector surface is then $P_1\ \Omega_1\ /4\pi$. If B is the brightness of the lamp, i.e. the produced power irradiated per unit solid angle per unit area, we have the relation

$$\frac{\Omega_1}{4\pi}\ P_1 = B\ \Omega_1\ dS_1 \qquad (4.1)$$

The brightness is, however, constant in a diffraction limited system (if absorption losses are neglected). Thus, if 1 denotes the lamp and t denotes the target,

$$P_t = B\ \Omega_t\ dS_t \qquad (4.2)$$

$$\frac{P_t}{dS_t} = \frac{P_1\ \Omega_t}{dS_1\ 4\pi} \qquad (4.3)$$

The interesting thing is to compare the irradiance at the target with the background light level. This irradiance is just proportional to the radiant emittance of the light source and the solid angle covered by the reflector as seen from the target.

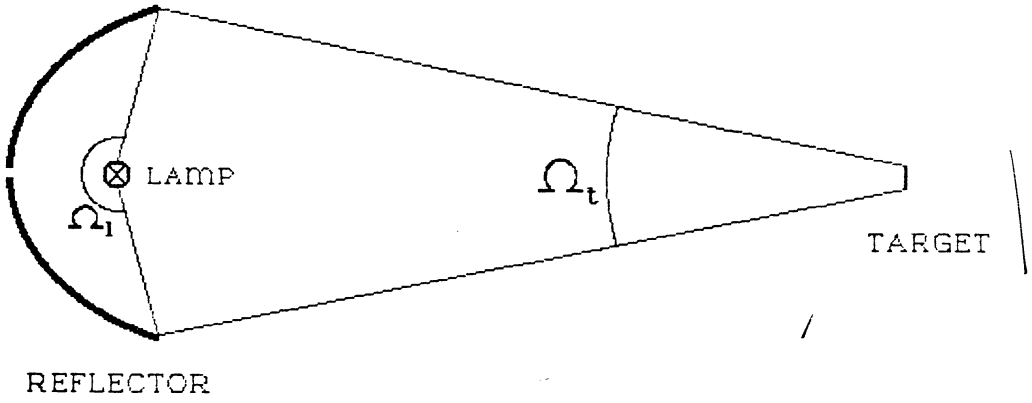

Fig 4.1: A schematic draft of the transmitting system, including some parameter definitions.

However, if aberrations also are included, the irradiated target surface dS_t will increase and thus the irradiance will decrease. For a spherical reflector used paraxially, the spherical aberration is the totally dominating aberration. According to Ref. [8] the divergence angle depending on this effect is

$$\theta_d = \frac{1}{256}\left[\frac{\Phi}{f}\right]^3 \qquad (4.4)$$

where Φ is the diameter of the reflector and f is its focal length. For a reflector with high light collection efficiency the spherical aberration can be shown to drastically influence the image spot size. A parabolic reflector with reasonably small manufacturing tolerances should be preferable.

The type of discharge lamp has to be considered in specifying dimensions of the reflector. In practice, for deep parabolic reflectors, the discharge has to be directed along the optical axis. Assume then the emitting volume to be a fine cylindrical volume on the optical axis. A ray-tracing calculation can be performed where the incident and reflecting angles are considered. This calculation is briefly treated below.

Since the incident and reflected light angles are equal (the law of reflection), the scalar products for the normalized vectors with the normal to the reflector surface will be equal to each other

$$\frac{\bar{X} - \bar{X}_l}{\left|\bar{X} - \bar{X}_l\right|} \cdot \bar{n}(X) = \frac{\bar{X} - \bar{X}_t}{\left|\bar{X} - \bar{X}_t\right|} \cdot \bar{n}(X) \qquad (4.5)$$

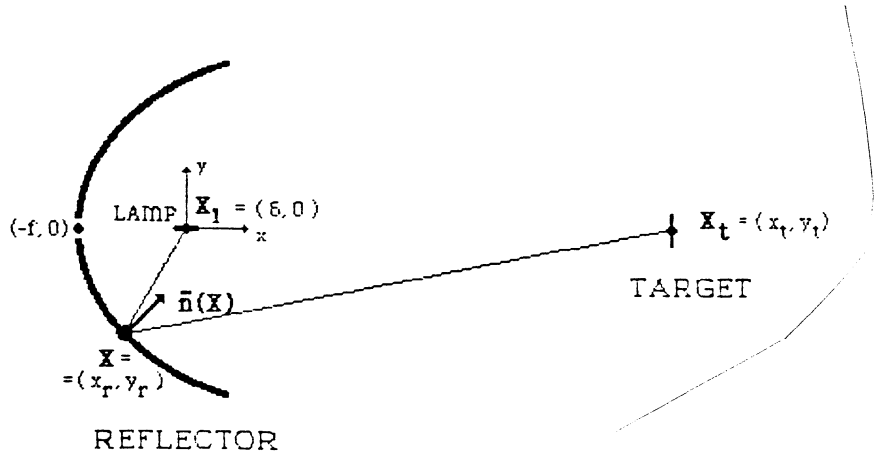

Fig 4.2: The coordinates of some arbitrary points at the lamp, reflector and target.

Eq. (4.5) is thus the relation for equal incident and reflected angles in the mirror. $\bar{n}(X)$ is the surface normal in the coordinate point X. Because of the symmetry in the calculations only $y_r > 0$ need to be considered. A signshift of y_r just causes a signshift of y_t. With the assumptions that

$$x_t \gg f, y_r$$

$$|\delta| \ll f, y_r$$

light emitted in a point $(\delta,0)$, reflected in a focal-length f reflector at the radius y_r is striking the target at a distance x_t approximately at the spot radius y_t

$$y_t = y_r \left[1 - \frac{16f^2 x_t \delta}{16f^4 + 8f^2 y_r^2 + y_r^4} \right] \qquad (4.6)$$

The interesting point, however, is to reach an expression for the irradiance, or power per unit area, at the target. To get a high irradiance a small spot and a high collection efficiency are needed. To get a small spot y_t has to be small for all $\delta_1 < \delta < \delta_2$ and for all $0 < y_r < y_{r,max}$, where δ_1 and δ_2 are the x-coordinates for the ends of the fine cylindrical lamp. There are two terms in eq. 4.6 giving rise to the image spread. The first one originates from an infinitely small source emitting light, which is reflected as a parallel output beam, while the other one is caused by the divergence of the light depending on the finite dimension of the lamp. The divergence depends

heavily on the focal length of the reflector as well as where in the reflector the light is reflected. A longer focal length will cause less divergence but will also demand a larger reflector diameter to keep the same collection efficiency.

The number of variables in eq. 4.6 is large and a numerical solution for different parameter combinations is presented in Fig. 4.3.

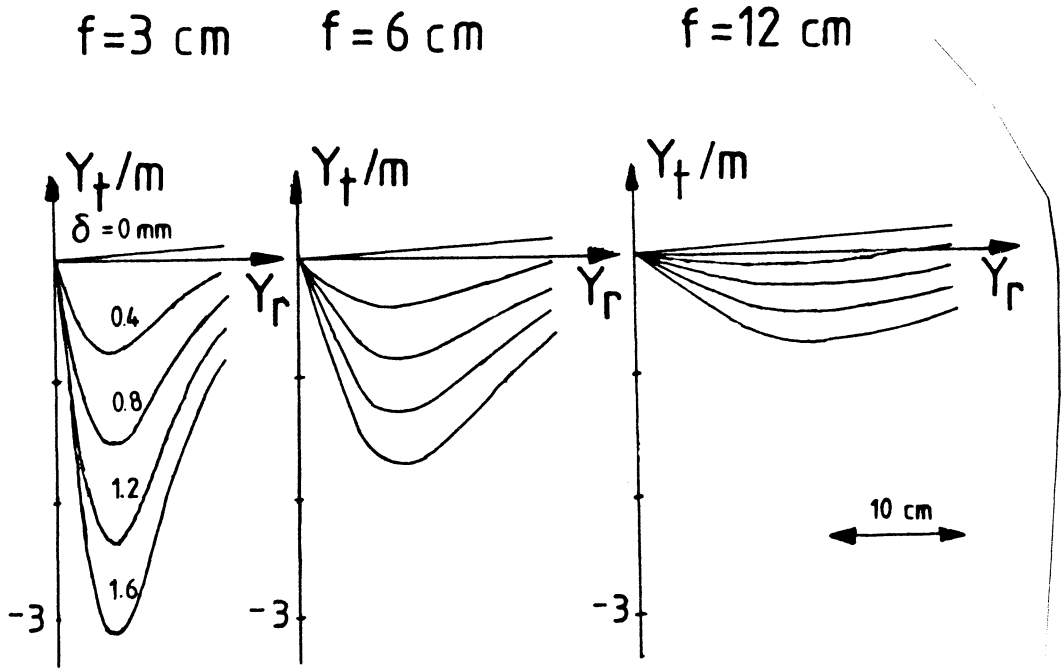

Fig. 4.3: *$y_t = y_t(y_r)$ for different δ and f. The curves in the two rightmost diagrams have the same δ values as the corresponding curve in the left diagram.*

In eq. 4.6 y_t is an odd function of y_r. The target spot diameter can therefore be defined as $2|y_t|_{max}$, where $|y_t|_{max} = |y_t(f,\delta)|_{max}$ is taken from Fig. 4.3. As can be seen in the figure, δ=0, i.e. the focal point of the reflector, is not always the point that yields the smallest target spot. It is then possible to get a smaller image of the lamp by focusing. The improvement in spot size by focusing is especially clear for large reflector focal lengths.

An analytical solution giving the reflecting radius yielding the largest taget spot can easily be found if any of the two terms in eq. 4.6 are small and neglible compared to the other. If the second term is in excess and the spot size therefore is determined by the divergence, a derivation of eq. 4.6 gives an expression for the reflecting radius causing the light to strike the edge of the target spot.

$$\frac{dy_t}{dy_r} = \frac{16x_t\delta\left[16 - 8\left[\frac{y_r}{f}\right]^2 - 3\left[\frac{y_r}{f}\right]^4\right]}{f^2*\left[16 + 8\left[\frac{y_r}{f}\right]^2 + \left[\frac{y_r}{f}\right]^4\right]^2} = 0 \qquad (4.7)$$

$$\Longrightarrow \quad \frac{y_r}{f} = 1.15$$

In this case the spot radius becomes

$$y_{t,max} \approx \left| 0.65 \frac{x_t\delta}{f} \right| \qquad (4.8)$$

The power reaching this spot area is approximately the optical power from the lamp integrated with the transmission function for the filters times the collection efficiency of the reflector.

$$P_t = \frac{\Omega_1}{4\pi} \int_{\lambda_1}^{\lambda_2} P_l(\lambda)\, t_f(\lambda)\, d\lambda \qquad (4.9)$$

where $P_l(\lambda)$ is the power per wavelength interval of the discharge lamp and t_f is the filter transmission function. To be able to calculate P_l, Ω_1 has to be expressed in known parameters.

$$\Omega_1 = \Omega_1' - \Omega_1''$$

where Ω_1'' is the half angle of the inner hole of the reflector and Ω_1' is the solid angle of the reflector seen from the lamp (Fig. 4.4).

$$\begin{cases} \Omega_1' = 2\pi(1 - \cos\theta') \\ \Omega_1'' = 2\pi(1 - \cos\theta'') \end{cases}$$

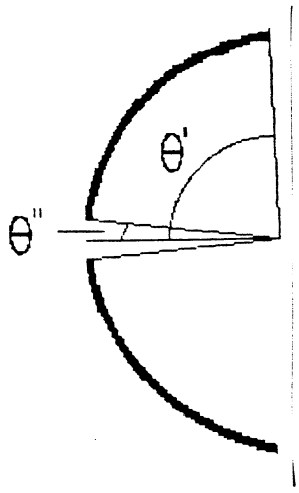

Fig 4.4: The reflectors available have inner holes which cause reductions of the the resulting solid angles. A reflector is shown and angles are defined.

Manufacturer	Model No.	Focal-length f (cm)	Reflector diameter Φ (cm)	Collection efficiency (C.E.)	$y_{t,max}$ (m)	C.E./ $y_{t,max}$ (m^{-1})
Pichel Industries Inc.	P6-2	3.25	24.0	0.67	4	0.2
-"-	P7-2	12.5	65.0	0.58	0.8	0.7
-"-	P8-5	5.88	35.3	0.64	2	0.3
-"-	P9-2	17.3	75.0	0.49	0.4	1.2
Lichtenknecker Optics, spherical		100.0	30.0	0.005	0.01	0.5
Edmund Scientific H80,254		12	45.0	0.5	0.9	0.6
Standard H4 car reflector		3	16	0.5	4	0.1

Table 4.1: Some commercially available reflectors with data. Column 5 and 6 are calculated according to eq. (4.6) with x_t = 100 m and δ = 1.5 mm. All reflectors are paraboloids, but the Lichtenknecker Optics one, which is sperical. The last column gives a relative value for how useful the reflector can be in a system (cf. eq. 8.1).

Since the discharge is approximated with an infinite fine cylinder and since the calculations have not considered intensity variations inside the irradiated spot the result can only be a rough approximation of the light irradiation at the target.

Reflective coatings.

Since a broadband reflectivity is wanted in the ultraviolet region a metallic coating is to prefer compared to a dielectric one. A-quarter-of-a-wavelength thick layers are sandwiched on each other to make a dielectric mirror. A mirror with a broadband reflectivity in the UV region thus needs to have a complicated multilayer structure with thin dielectric layers. Metallic reflectors can, however, quite easily be manufactured with high reflectivity far out in the ultraviolet region. Aluminum is the most widely used metal for reflecting films, offering consistently high reflectance throughout the visible, near-infrared and near-ultraviolet parts of the spectrum. To increase the performance in the ultraviolet part of the spectrum, the surface can be overcoated with a quarter wavelength thick ultraviolet transmitting film. This dielectric layer (usually MgF_2) not only increases the reflectivity but it also prevents oxidation of the aluminum surface and provides abrasion resistance. An even more resistant reflecting film is rhodium. Rhodium is resistant to oxidation and tarnish, even at high temperature, and it is exceptionally hard and durable. It also adheres well to nickel substrates, which is preferable for a large parabolic reflector. The reflectivity is however less than the reflectivity for UV enhanced aluminum (Fig. 4.5). The rhodium film can be either electrolytically deposited or evaporated on the substate. The reflectance as well as the surface accuracy is slightly better for an evaporated film, but it is much easier to produce the deep paraboloids with electrolytical deposition.

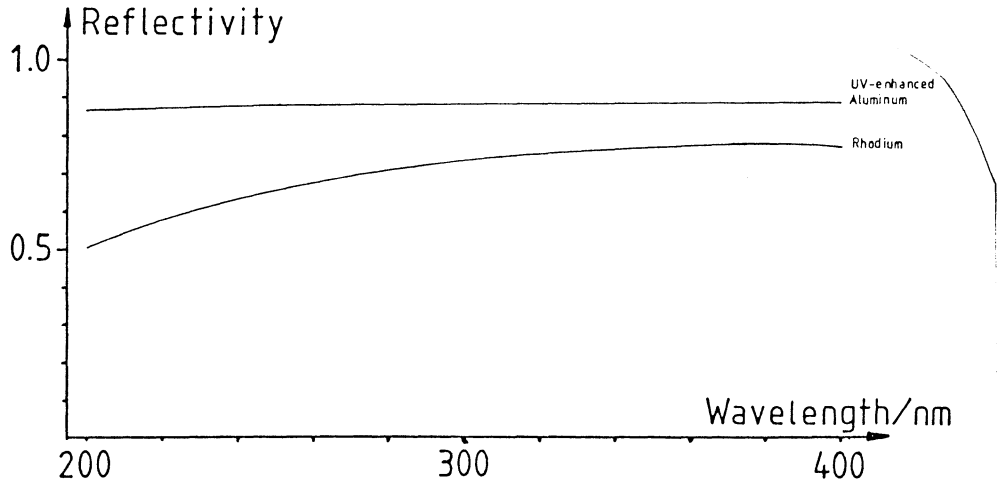

Fig 4.5: Reflectivity for UV enhanced aluminum and for rhodium.

5. LABORATORY TEST

Spectra for a filtered xenon flashlamp (Noblelight SAPX 10015) were captured with an EG&G PAR OMA 2 optical multi-channel analyzer Model 1215 with a Model 1420 diode array detector in the focal plane of a Jarrell-Ash Monospec 18 spectrograph. Different UV-transmitting filters were used in order to suppress lamp wavelengths in the region of interest for fluorescence detection. This is due to the necessity of distinguishing between the fluorescence and the elastically scattered light.

To select suitable wavelengths for fluorescence detection, spectra of some relevant oil samples were recorded in the laboratory with the set-up shown in Fig. 5.1. As a light source the xenon flashlamp was used. For each flash 200-400 mJ of electrical energy was discharged in the lamp. Some of the light was collected with a Φ=9.5 cm, f=15 cm quartz lens and filtered with a Schott UV-transmitting filter. About 0.01% of the electrical energy discharged reached the sample as UV-light. The overall conversion efficiency of the lamp was a few (<5) per cent. The fluorescence light was collected by means of another

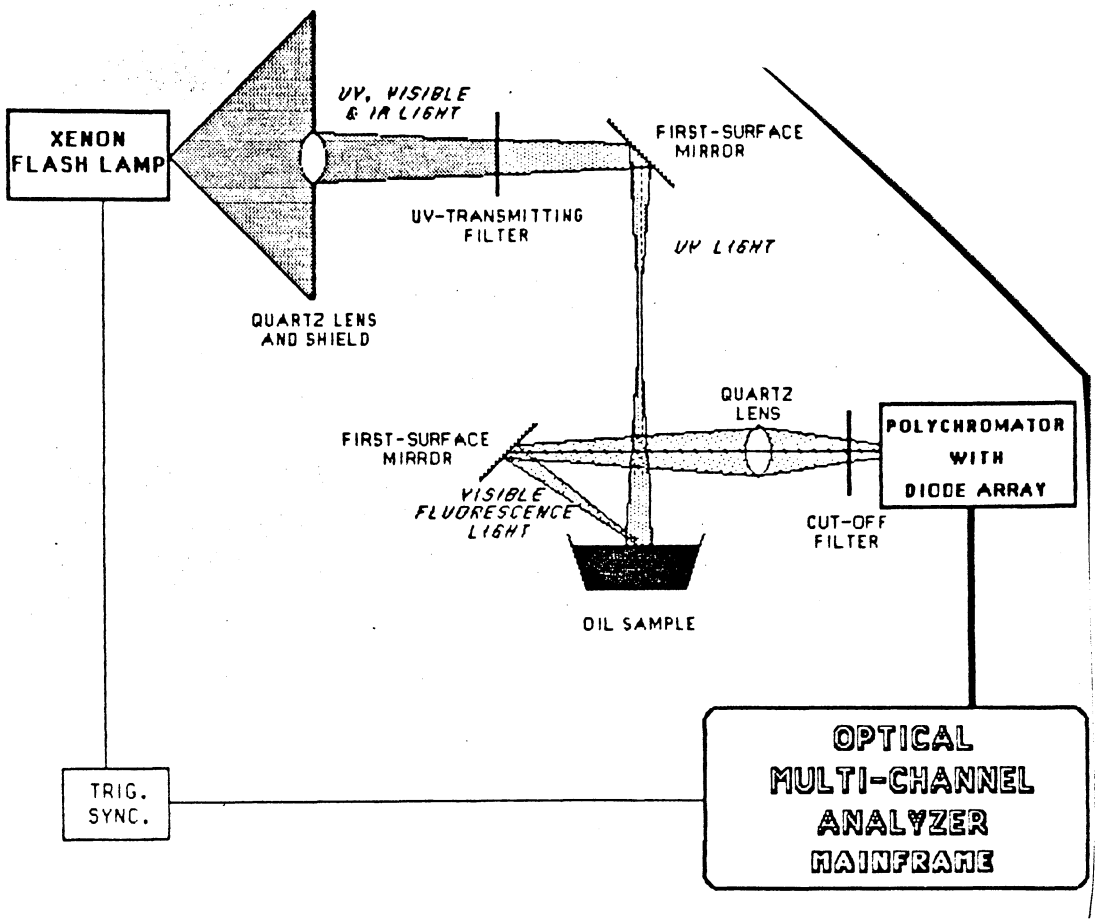

Fig. 5.1: Laboratory set-up.

quartz lens and filtered with a Schott cut-off filter to suppress elastically scattered UV-light before it entered the detection system. Different combinations of UV-transmitting and cut-off filters were tested. When capturing the spectra in Fig. 5.3 a Schott UG 1 UV-transmitting filter (Fig. 5.2) and a Schott GG 400 cut-off filter were used. The detection system was the EG&G PAR OMA 2 system. The intensity of a specified layer thickness of a 70 µg/l solution of Rhodamine 6 G in water at its peak wavelength defines the intensity unit.

The internal transmission function of some Schott UG UV-transmitting filters can be seen in Fig. 5.2. Some relevant oil spectra are shown in Fig. 5.3. These spectra are very similar to those of the same oils in Ref. [1], where a nitrogen laser was used as the exciting light source. This is in accordance with theory. The spectral distribution of the fluorescence light is with few exceptions independent of the excitation wavelength as long as this wavelength is short enough to excite the molecule [9].

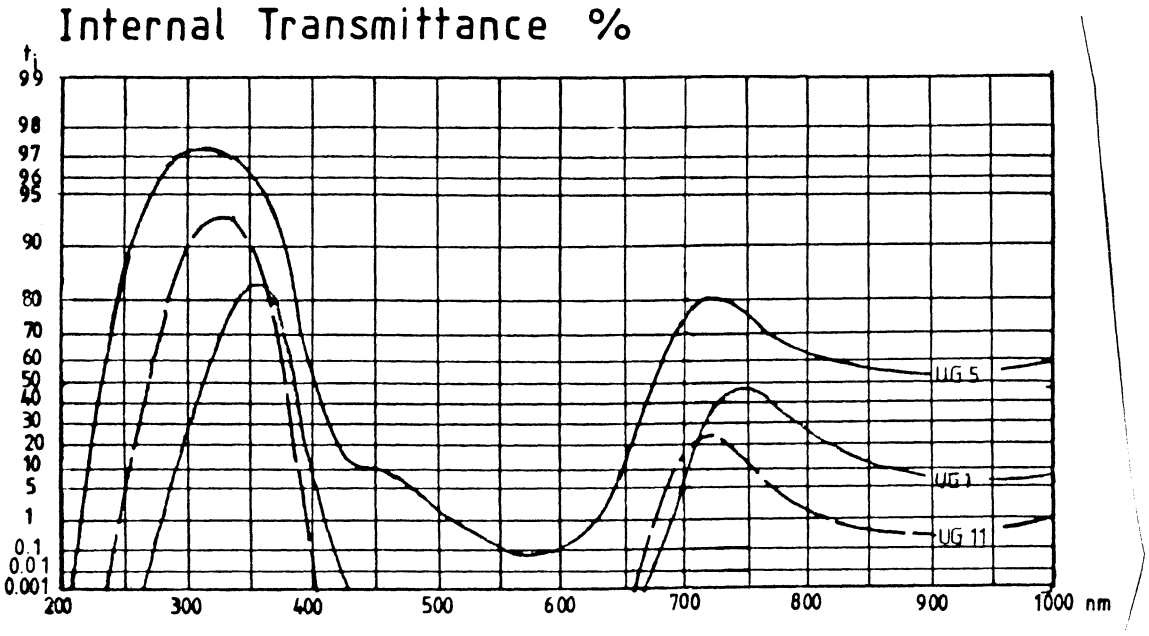

Fig. 5.2: Transmission of some relevant Schott UG filters.

Intensities at three selected wavelengths are given for the different oils in Table 5.1. To distinguish between the oil types the intensities at these wavelengths can be measured and ratios between them formed. The reason for comparing wavelengths by forming ratios is, as pointed out in Ref. [10], that a dimensionless ratio is insensitive to target distance changes, lamp output fluctuations and target topography variations.

OIL PRODUCT	INTENSITY AT			RATIOS	
	A 436 nm	B 465 nm	C 525 nm	A/B	B/C
Statford Crude	13	14	15	0.93	0.93
Brent Crude	10	13	14	0.77	0.93
Heavy Fuel Oil E410	2.9	4.9	7.4	0.59	0.66
Heavy Fuel Oil E510	2.7	4.6	7.0	0.59	0.66
Fuel Oil 1 (Diesel)	81	47	13	1.72	3.6

Table 5.1: Intensities at different wavelengths for the oils in Fig. 5.3 and some relevant intensity ratios.

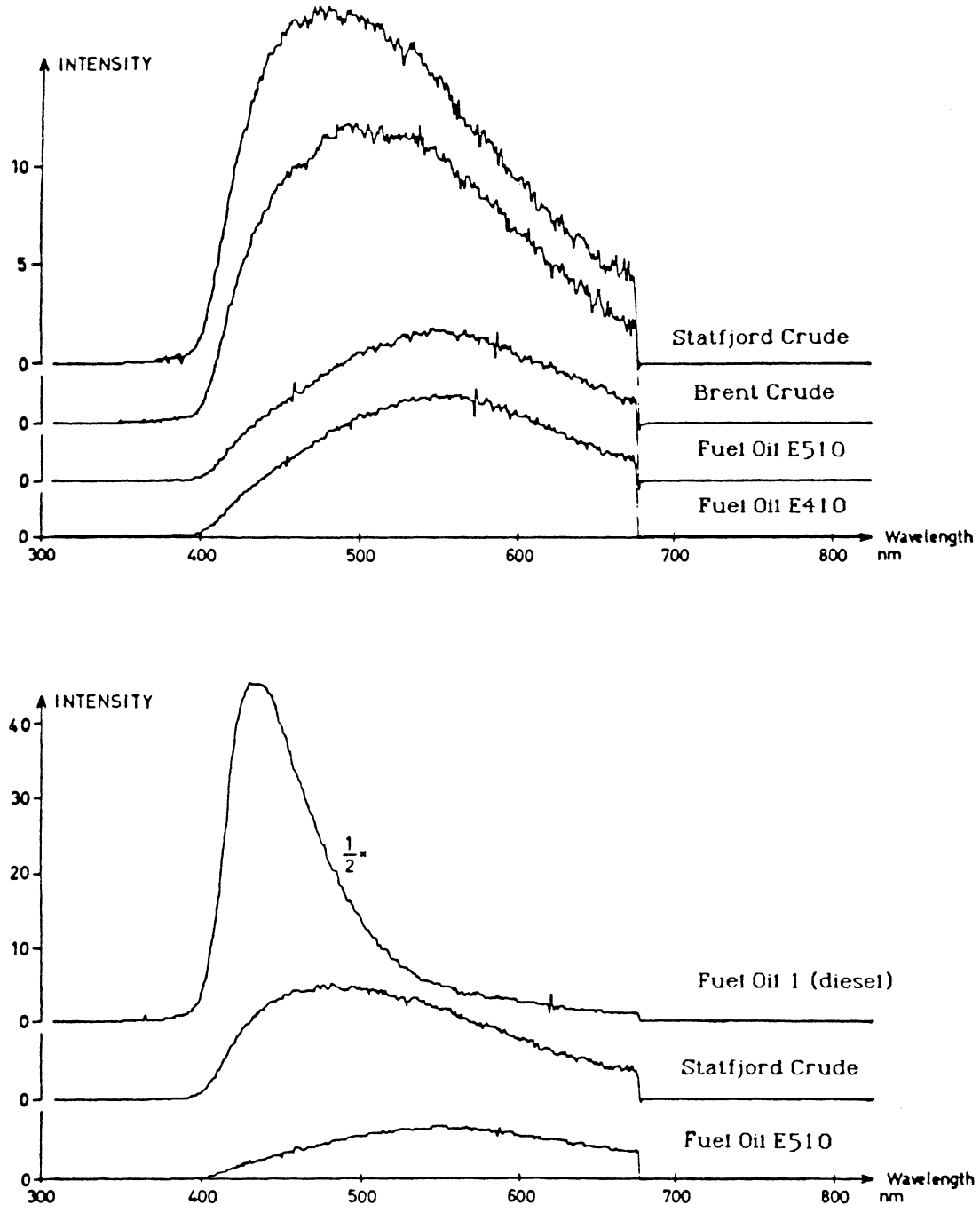

Fig. 5.3: Spectrally corrected fluorescence spectra of different oil products, the fluorescence being induced by the lamp light filtered through a UG 1 filter.

6. FIELD TEST

The range measurements were performed outdoors through an open window under the same experimental conditions as in the measurements presented in Ref. [1]. The optically thick oil samples were placed on an aluminum foil on the roof of a building about 70 m away and the

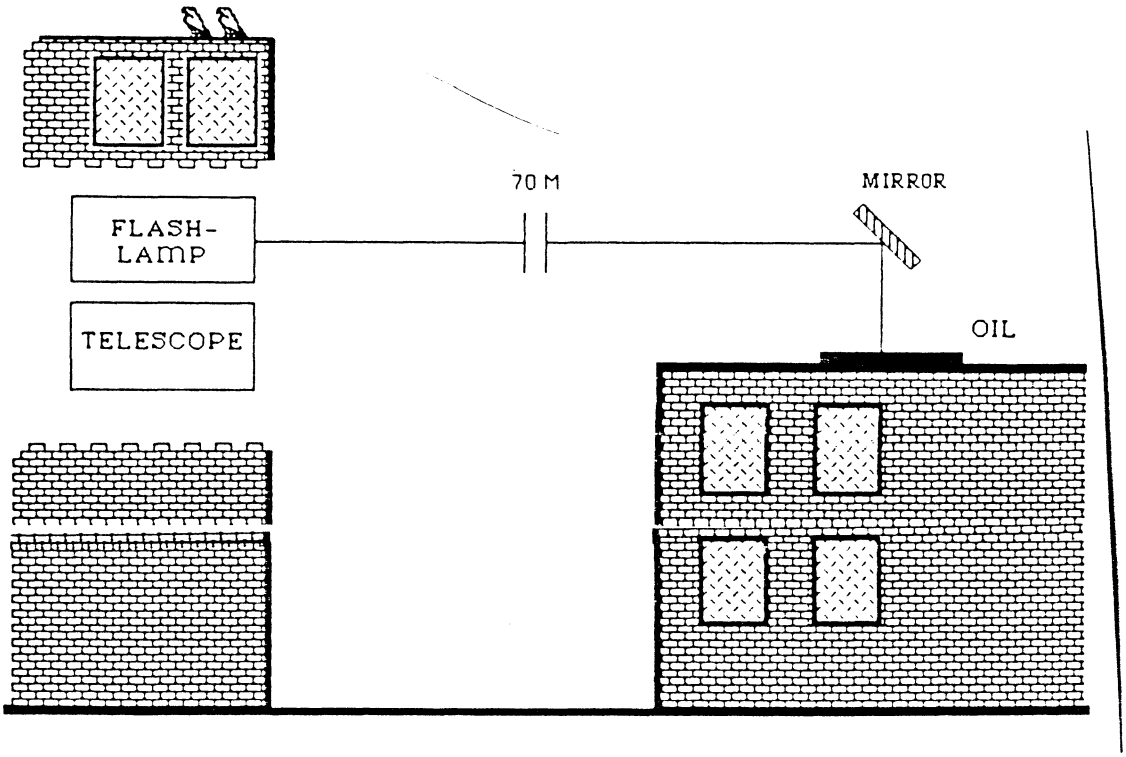

Fig. 6.1: Range overview.

light was deflected down on the sample by a large mirror as can be seen in Fig. 6.1. The experimental set-up is shown in Fig. 6.2. The lamp used was the same xenon flash lamp as in the laboratory tests (Noblelight SAPX 10015). The signals were captured with an EG&G boxcar averager Model 4420 equipped with two Model 4422 integrators. Further, the signals were recorded and processed in a signal processor Model 4402. The waveform of the elastically scattered lamp light from the target can be seen in Fig. 6.3. The lamp had a pulse duration (FWHM) of about 20 µs. The lamp was generally operated at a frequency of 1.5 Hz with an electrical discharge energy of 10 J. The lamp light was filtered through a 2 mm thick Schott UG 11 filter.

To minimize the target spot size, the flashlamp was placed in an optimum point near the focal point of the reflector (cf. Fig. 4.3 and the discussion below the figure). Four reflectors were tested in the measurements, one UV-enhanced aluminum coated spherical reflector with focal-length f=100 cm and exit diameter Φ=30 cm (Lichtenknecker Optics) and three parabolic reflectors, one with f=12 cm and Φ=45 cm (Edmund Scientific), one with f=3 cm and Φ=16 cm (a standard car reflector) and one rhodium coated parabola with f=3.2 cm and Φ=24 cm (Melles Griot). The parabolas covered a considerably larger solid angle seen from the lamp than the spherical reflector did. For those reflectors it was impossible to place the standard size (5 cm x 5 cm) filters available around the lamp in such a way that all the lamp

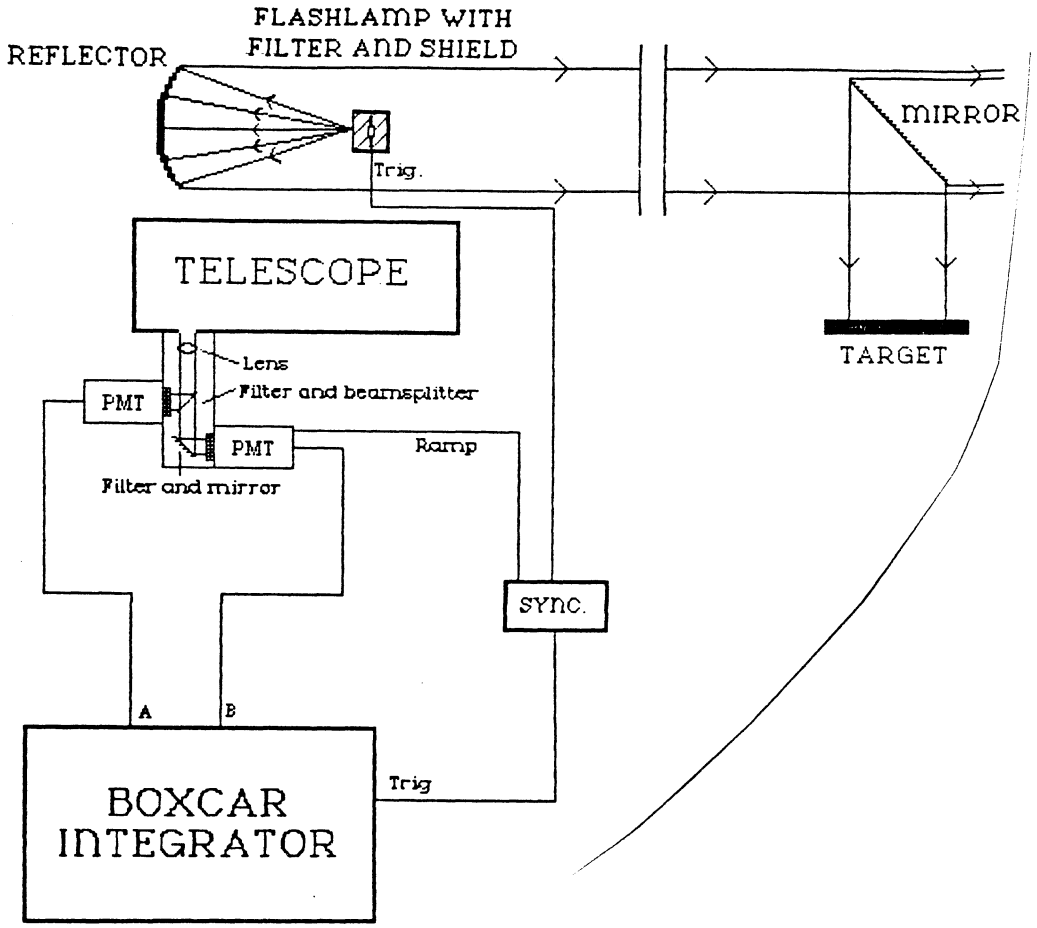

Fig. 6.2: Experimental set-up for range measurements.

light was filtered and still the entire reflector collection efficiency was utilized. Therefore the spherical reflector was chosen for the fluorescence measurements. The parabolic reflectors were tested to see how much the reflector choice can improve the target irradiation.

When using the spherical reflector, the lamp axis was placed perpendicularly to the optical axis, not to shade the reflector with the lamp electrode. This placement is important in the case of the spherical reflector, since it just covers a small solid angle seen from the lamp. The measured target spot size should not be compared with the theoretical calculations for this reflector, as the base for the calculations is a model with the lamp axis along the optical axis.

The fluorescence signal was collected with a 25 cm Newton telescope, and the collected light was formed to two beams by means of a positive lens and a beamsplitter (Fig. 6.2). In front of the two detecting photo multiplier tubes (EMI 9558QB and 9816QA, both with S-20 response), bandpass filters were placed. Three wavelength bands were studied, one in the violet (436 nm, with 15 nm bandwith and a peak transmission of 25%), one in the blue (peak wavelength = 458 nm, bandwidth = 10 nm and with a peak transmission of 40%) and one in the green region (peak wavelength = 525 nm, bandwidth = 5 nm and with a peak transmission of 55%) by changing filters. The PMT signals were recorded with the boxcar integrator. In our presentation all signals

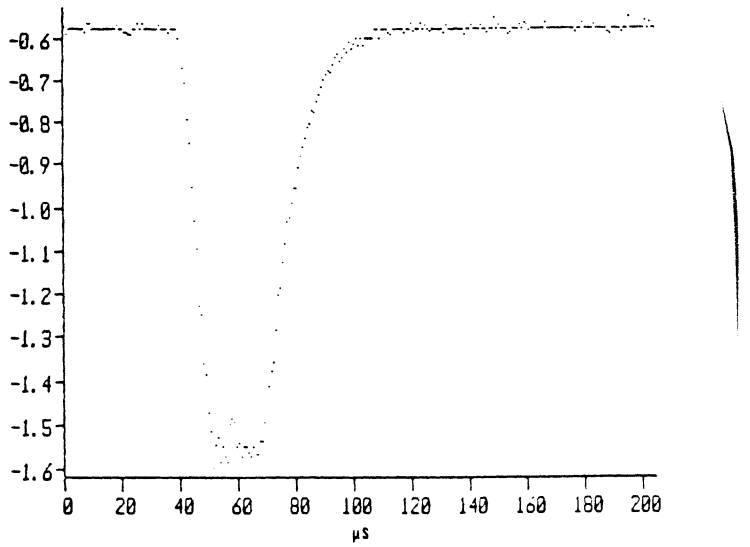

Fig. 6.3: The lamp waveform recorded in the transient time domain.

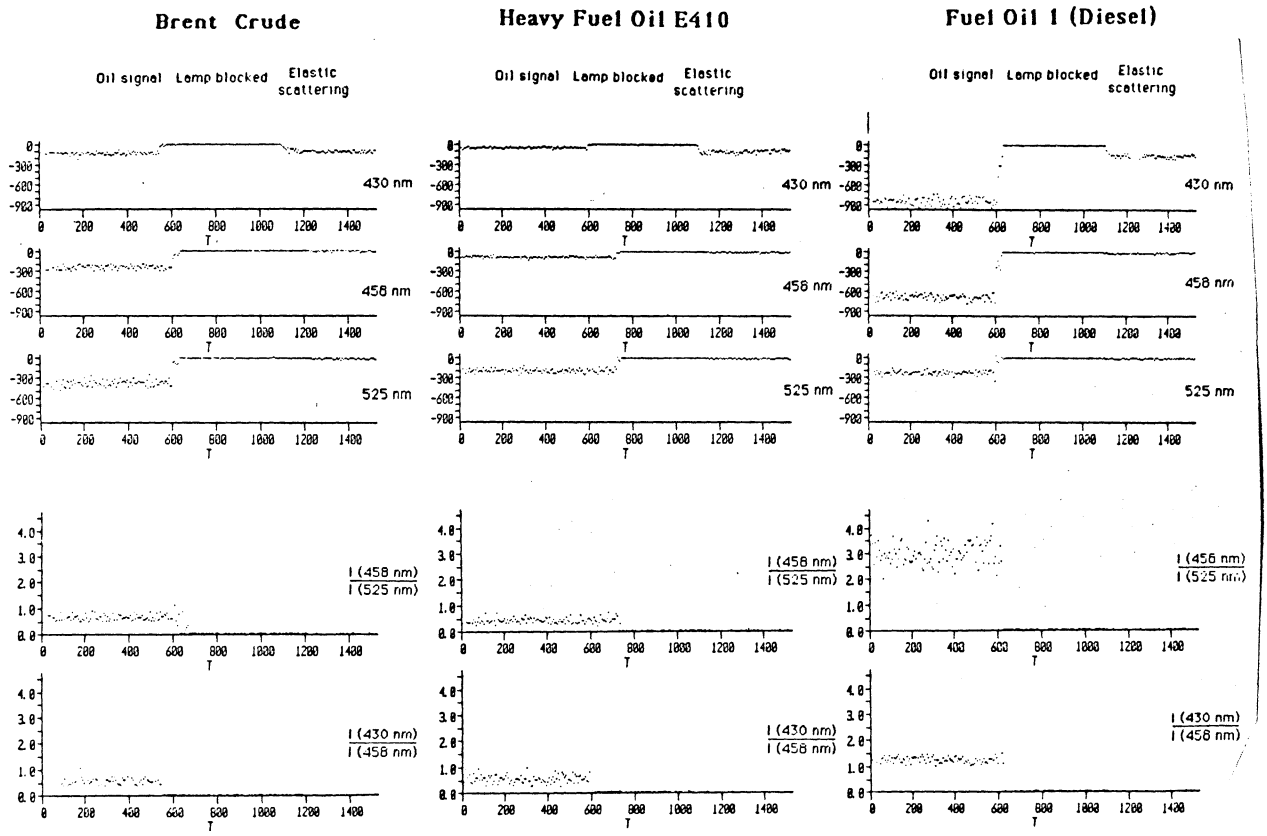

Fig. 6.4: Recordings for different oils made during night time with the boxcar integrator. Intensities were captured at 436, 458 and 525 nm. At each recording the intensity from the oil was measured first, then after about 600 trig pulses to the boxcar, at T≈600, the exciting light was blocked and the background level recorded. An aluminum foil was placed as a target. At T≈1100 the lamp light was unblocked again and the level from the non-fluorescing aluminum was measured. 6 shots were averaged for each measuring point. Ratios between the recordings are shown as well. As soon as any of the signal levels is too small, the uncertainty in the diagnostic is high and no significant result can be achieved. The ratio is unsignificant and can be electronically rejected. That is done to the right in the ratio curves.

are negative, since the detectors are photomultiplier tubes, and all real zero levels (no detected intensity) are placed at zero on the vertical axis in the figures.

During the work difficulties in filtering the lamp properly were experienced. A 2 mm thick Schott UG 11 UV-transmitting filter was required to get a sufficient suppression in the spectral range where detection was to be performed. The part of the lamp output that did not reach the reflector had to be carefully shielded since even small amounts of stray light in the visible region influenced the measurements.

During nighttime, when the background light level was low, recordings were made for the different oil types. If the signal levels were significant, ratios between the signal levels for the three wavelengths studied were calculated. The gate width was 10 µs and 6 samples were averaged for each of the 256 measuring points. The lamp was flashed for every other trig pulse to the boxcar. The other trig pulse was used to measure the background.

The horizontal scale (T) in Fig. 6.4, in which the recordings are shown, is the number of trig pulses to the boxcar. For each oil, the fluorescence intensity was measured first, then, at T≈600, the lamp was blocked and the background intensity due to noise was recorded. During this time interval an aluminum foil was put at the target place. At T≈1100 the lamp was unblocked again and the level of the light scattered towards this foil was captured. The deviating correspondence between the oil fluorescence intensity ratios obtained

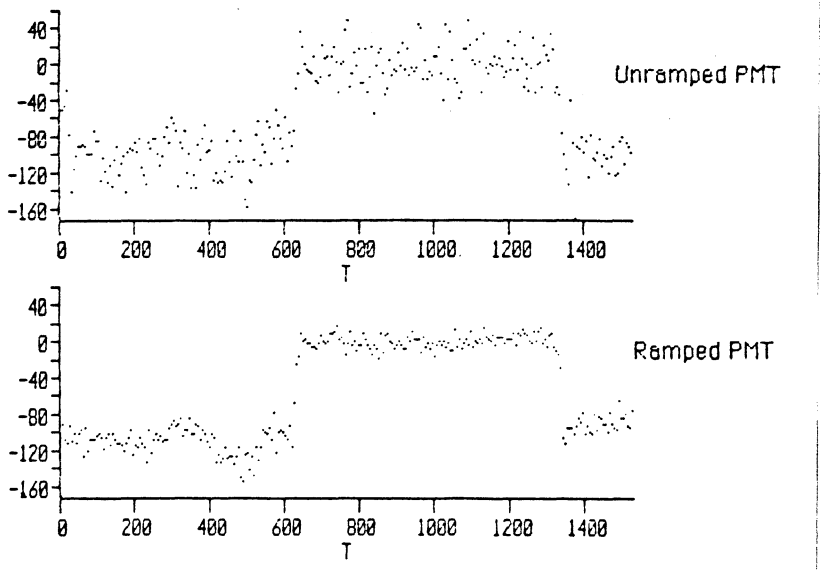

Fig. 6.5: An integrating daytime recording of the 436 nm fluorescence from the diesel oil for the two PMT's used. The recordings were made with the lamp transmitted the first 600 trig pulses, then the lamp was blocked between T=600 and T=1200 and then transmitted again.

here and those in Table 5.1 can be explained by the non-flat spectral response of the PMT:s. For all oil types the violet signal level seems to be too high. This can be explained by a finite suppression by the UG filters for this wavelength. The transmission tail at 400 nm, which can be seen in Fig. 5.2 , causes some elastically scattered light to be detected that is added to the fluorescence signal. The oil fluorescence was recorded also during daytime (in cloudy weather) for the strongest fluorescing oil, the diesel oil, at 436 nm. This yielded a signal to noise ratio of 5:1. Curves from the two PMT:s used are shown for this oil fluorescence in Fig. 6.5. A separate measurement yielded that in December the background irradiance is about 10 times higher on a bright sunny day than during this conditions.

At daytime a higher background light level limits the maximum possible high voltage on the PMT:s. A higher voltage over the dynodes will yield such a high dc current from the PMT due to the constant light level, that the PMT anode will be destroyed. If a background is present, one has to assure that the right background is subtracted from the signal. This can be done with a second gate opened just after the fluorescence signal has ceased. The two gates should not be separated more than the experimental circumstances require. The importance of background subtraction is clearly seen in the Fig. 6.6.a and 6.6.b recordings. In Fig. 6.6.a two recordings are shown, with and

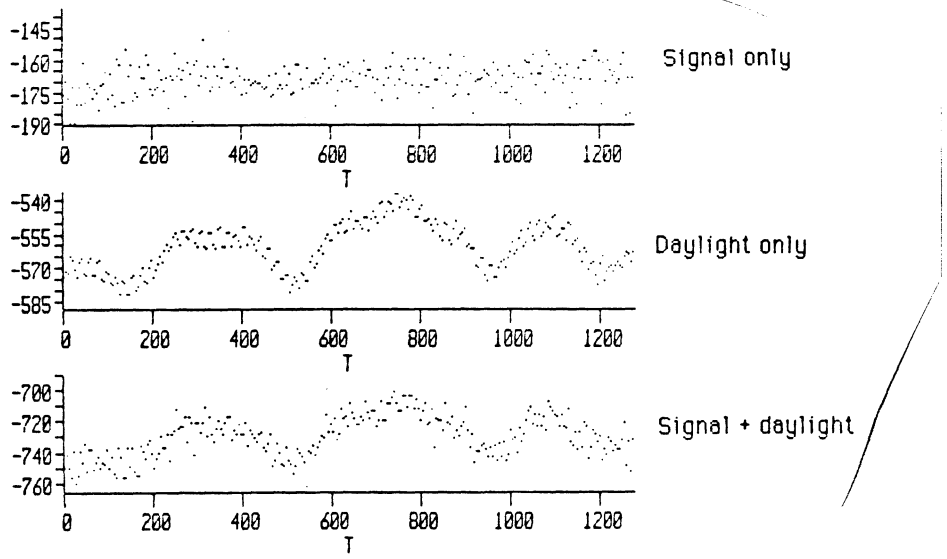

Fig. 6.6.a: Integrating recordings made with two photomultipliers during daytime. The gate in the middle curve was delayed 64 µs after the one used for the lower one and captured no fluorescence signal. The upper curve is the middle one subtracted from the lower one, hence eliminating daylight influence. The scale is enlarged to show the structure of the noise, but still with the real zero level placed at zero on the vertical axis.

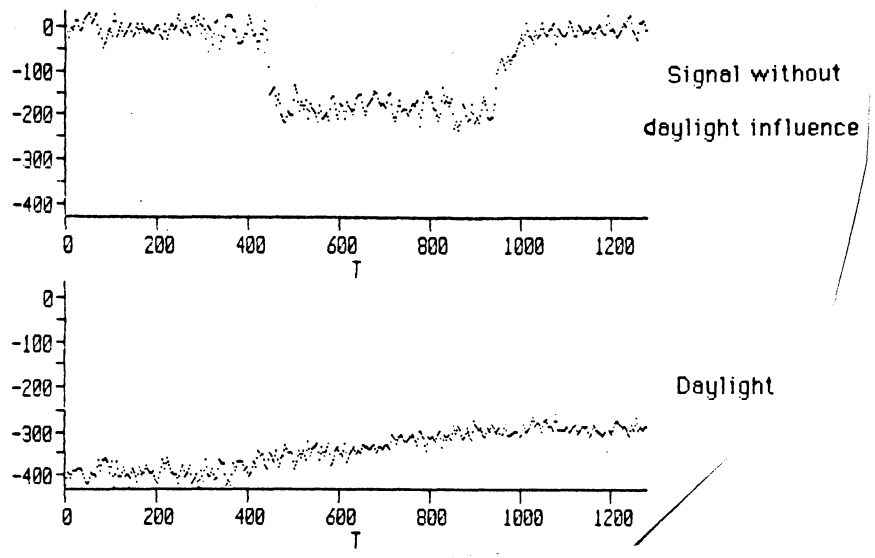

Fig. 6.6.b: Gated integrator recordings showing daylight influence. The lamp is transmitted in the middle of the curve, while it is blocked to the left and to the right.

without signal added to the daylight background. The second recording was made with the gate pulse delayed 64 µs after the first one. The difference between the two recordings is shown as well. This is the signal "lifted off" the background. In Fig. 6.6.b the same thing is demonstrated. The lower curve is a recording of the background only. Between T=0 and T=400 and between T=1000 and T=1200 the exciting lamp light was blocked, showed in the signal curve above.

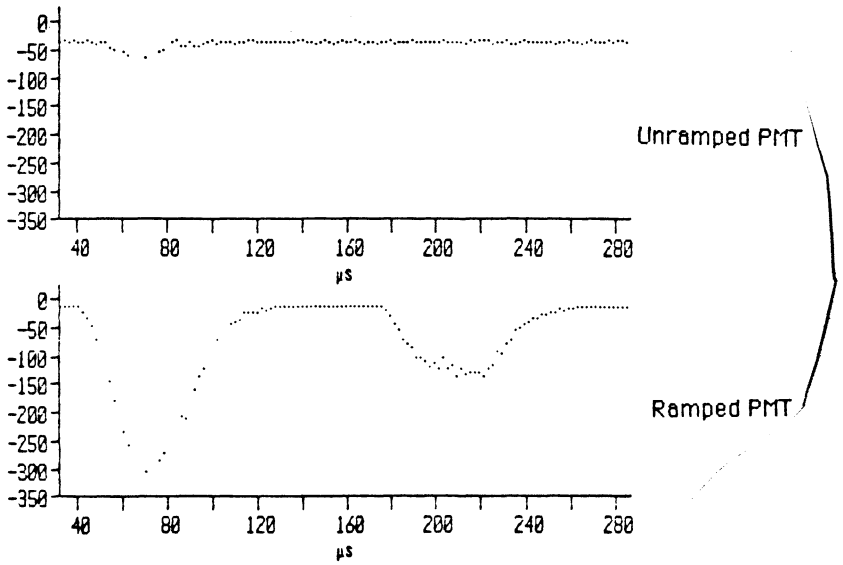

Fig. 6.7: Transient signal recordings in the presence of normal daylight with a ramped and a non-ramped photomultiplier. The upper curve shows the signal waveform on a constant background light level captured with the unramped PMT. The lower curve is a recording made simultaneously with the ramped PMT, showing two ramps with the signal waveform superposed on the background in the first ramp. The second ramp captured the background only and can be used to subtract this.

One way to circumvent the problem with the flowing dc current through the PMT is to gate or ramp it. This means that the high gain is switched on only during a short time period at the sample point, i.e. during (and for the background immediately after) the lamp flash. It will not cause a higher fluorescence signal compared with the measured background level, but it will allow a higher gain in the PMT, without anode burning. This is often preferable since the PMT usually has a lower noise level than other amplifiers. A softly ramped PMT, modified at our department, was tested. The ramp was softly adapted not to cause the output current to oscillate. Two sets of recordings comparing the ramped PMT, the EMI 9816 QA, with a common one (EMI 9558 QB) are shown in Figs. 6.7 and 6.8. Fig. 6.7 shows two recordings in the transient time domain, like it looks on an oscilloscope, showing the signal waveform and the ramps of the ramped PMT, while Fig. 6.8 compares gated integrator recordings. The second ramp in Fig. 6.7 can be used for background light subtraction. On the occasion of these recordings a constant light flow (from the daylight) reached both PMT:s.

Measurements comparing the signal to noise characteristics of the two PMT:s in daylight were also performed and the results are presented in Fig. 6.8. Here, the daylight put a limit to the voltage that could be applied to the non-ramped PMT. No better signal to noise ratio could be achieved with ramping on the boxcar used, as can be seen in the figure. However, the ramped PMT (EMI 9816QA) showed a better dark current characteristic, causing a lower noise when no or little background light was present, than the unramped one (EMI 9558QB) did. Most of the advantages gained with ramping a PMT in this application, is to get a high signal level to the boxcar A/D conversion. This is important, since the digital representation requires a high value to get a good resolution. But the boxcar used already has a very high resolution, so even if the fluorescence signal only was some per cent of the total detected signal, it could be significantly recorded.

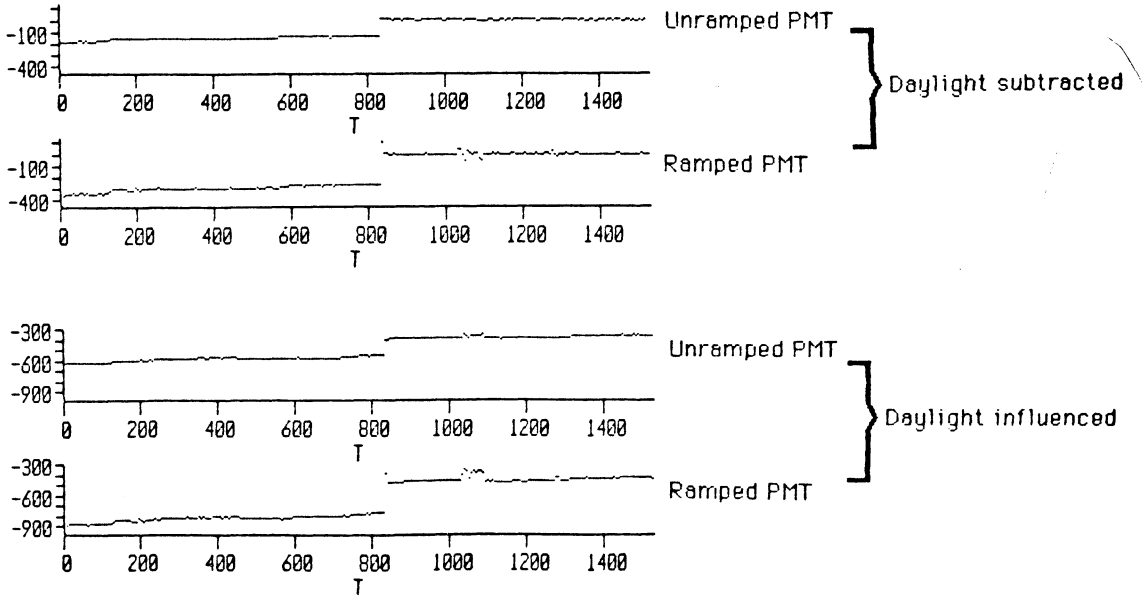

Fig. 6.8: Integrated fluorescence signals measured in daylight with the ramped and the unramped PMT. The lamp was blocked for T>850. The daylight is subtracted in the two upper curves.

In Fig. 6.9 the advantage of forming ratios in these types of measurements is clearly seen. At this time the light intensity reaching the target varied heavily due to fluctuating lamp output and varying transmission of the atmosphere because of fog. The intensities recorded with the two PMT:s is seen to fluctuate heavily, but the ratio is constant.

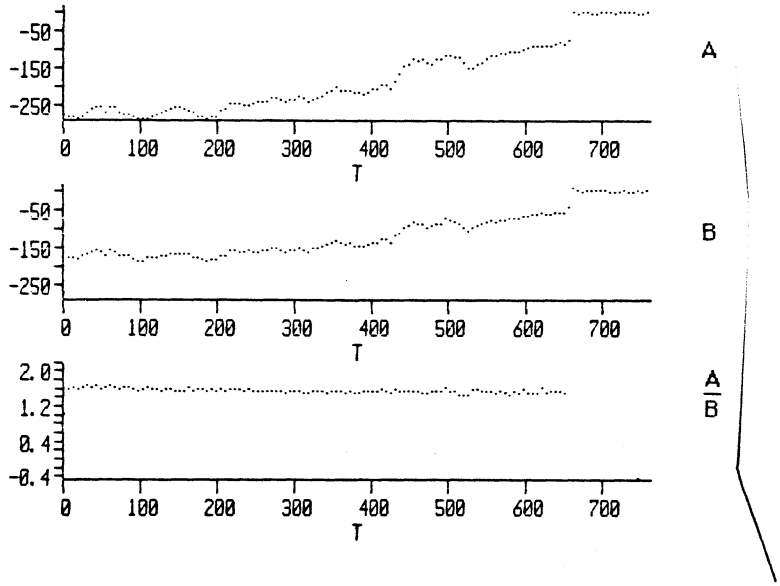

Fig. 6.9: Varying fluorescence signals due to atmospheric transmission fluctuations. The ratio is constant.

To determine the irradiance obtained at the target for different reflectors, the target spot size from an unfiltered lamp was measured. Three different reflectors were used, and the results can be seen in Table 6.1. The f=12 cm, Φ=45 cm parabolic reflector had a somewhat unsmooth surface and only the other two should be compared to the theoretical calculations in Chapter 4.

Reflector shape	f (cm)	Φ (cm)	Spot diameter as measured (m)	Spot diameter theoretical (m)
Parabolic	12	45	2.5	0.5
Parabolic	3	16	3	3
Parabolic	3.3	24	2.5	2.7

Table 6.1: A comparison between measured and calculated values for the spot size at 70 m target distance. The surface of the large parabolic reflector was somewhat unsmooth, and the measured value for this one does not agree very well with the theoretical calculations.

7. DISCUSSION

This investigation should be compared with the one presented in Ref. [1]. The fluorosensor treated in that work was based on a laser as inducing light source, but otherwise the experimental circumstances were the same.

In a comparison between a laser and a flashlamp, the flashlamp has a high conversion efficiency and the pulse energy can therefore be high with a small power supply and to a reasonably low price. To motivate the use of a laser in a measuring tool, the special laser light characteristics hence have to be preferable. In the case of exciting large molecules with wide energy bands, the monochromaticity of the laser light is not an advantage. The total UV-region between 200 and 400 nm can be used to induce fluorescence in all parts of the visible spectrum. However, the possibility to make short pulses and the parallel beam output of a laser are of great interest for the application discussed here, especially when the signal has to compete with background light (daytime operation).

During nighttime measurements only signal photons reach the telescope and will be detected. The signal level then only has to be compared with the electronic noise of the detection system. Neither a longer pulse nor a somewhat higher divergence will cause any problem. The fluorescence only has to be integrated for a longer time and the detection field-of-view has to be increased. In this situation, to a first approximation only the pulse energy will determine the signal to noise ratio. The recordings shown in Fig. 6.4 yield that it is possible to examine oils at a distance of 70 m with the set-up used. However, if the lowest recommended flying altitude of 300 m during nighttime is considered and the r^2-dependence of the fluorescence light is included in the calculations, the signal levels will decrease by a factor 20. On the other hand, the pulse energy reaching the oil slick could easily be improved by a factor 100 by selecting a reflector with a higher collection efficiency, cf. Table 4.1.

The situation in bright daylight measurements is much different. The signal photons now have to compete with the background light photons. The number of detected background photons is proportional to the filter transmission width, the detection time and the detection field-of-view. It is therefore desirable to detect as many signal photons as possible per unit time and per unit steradian of detection angle. Since the number of detected background light photons per unit time can be expected to be Poisson distributed [11], the noise surviving the background subtraction has a standard deviation proportional to the square root of the total number of detected photons:

$$S/N \sim \frac{n_s}{\left[n_B + n_s \right]^{1/2}} \qquad (7.1)$$

where n_s is the number of detected signal photons and n_B the number of detected background photons. The only way to improve the signal to noise ratio for a given sample and detection distance, is to manipulate the light source and make sure that the detection is optimal. Three parameters of the light source are of interest: the pulse length, the divergence and the pulse energy.

To optimize the detection, three corresponding detector characteristics are of interest: the measuring time, the detection field-of-view and the filter transmission function. These three factors influence the signal to noise ratio in a similar way as long as the main noise source is the photon statistics and not i.e. electronic noise. If the detection field-of-view is increased, starting from a small value, the S/N-ratio also increases, since the number of signal photons and the number of background photons increase equally. Of course the field-of-view must not be increased to cover anything but the illuminated spot. The same argument goes for the gate width. A gate width that is considerably smaller than the lamp pulse time means that fewer background photons are detected, but the S/N-ratio still is smaller than for a larger gate width, as can be inferred from eq. 7.1. For the same reason, the detection filter band widths should not be too narrow. However, if the band widths are so large that the transmission regions overlap, significant information is lost. A larger intensity reaches the photomultiplier when these measures are taken. This must of course be compensated with a smaller gain. This does not further increase the noise, though, since the detection system is operated far from its electronic noise level during daytime measurements.

The significance of ramping the PMT is not clearly seen in Chapter 6. The reason is the many digital levels of the analog-to-digital converter of the boxcar. It is important that the resolution of the detection system is so great that the result of a background subtraction still is a significant number. An alternative way of achieving this, instead of A/D-converting both the result of the first gate and the result of the second gate and then subtract them digitally, is to perform the subtraction analogically and then A/D-convert the result of this analog subtraction. Since a higher gain can be applied to a ramped PMT, the difference between the two gates is larger and thus yields a larger number of significant bits.

The signal levels have to exceed a certain value to be significant compared to the noise. Ratios between the signal levels for the three wavelenghts studied should be formed only if these values really are exceeded. If this is not the case, no conclusion of the oil type can be drawn.

For the flashlamp the long pulse and the relatively high divergence make it difficult to detect significant signal levels from oil during daytime. Fig. 6.5 shows recordings of diesel oil fluorescence captured on a cloudy day. As mentioned, a separate measurement comparing the background irradiance in bright daylight and a cloudy day yields a ten times higher background level in bright daylight than during the recordings in Fig. 6.5. In summer, however, the sun rises higher in the sky, causing a five times higher illumination on the latitudes of south Scandinavia than at winter solstice. Hence, despite a fifty times higher background light level than during the recording of Fig. 6.5, an acceptable signal-to-noise must be achieved.

Due to the long pulse time of a flashlamp, the time between the signal capturing and the background level recording also has to be long, of the order of µs. This means that a background that varies faster than this time can not be readily subtracted. Such a background is present on sunny days when the sea surface acts as a faceted mirror. This heavily fluctuating background can not be compensated for and that is one of the most serious drawbacks of a flashlamp system.

8. CONSTRUCTION CONSIDERATIONS

The detection system should consist of a mirror telescope, followed by photo multipliers and gated integrators. A telescope with a Cassegrainian configuration has the advantage of combining a long focal length with a compact construction. The telescope can be equipped with two interchangable exit apertures so that a larger field-of-view can be used at night time. The detection should be carried out in three wavelength bands and ratios of the intensities in these bands should be formed to eliminate the influence of fluctuating lamp power, varying atmospheric transmission, varying target distance etc. The background light should be subtracted from the signal by opening the gate again immediately after the signal has died off.

While the detection system configuration is clear and straightforward, the construction of the transmitting system is somewhat troublesome because of the many parameters.

The lamp should be operated in the simmer mode. Since most of the lamp light is UV-light between 200 and 300 nm, this wavelength region should be utilized for excitation, provided that suitable filters and reflector coatings can be found. The suppression in the detection region must be at least 10^6. An interesting filter in this application is the UV-transmitting fluid filter consisting of a mix of $CoSO_4$ and $NiSO_4$ solutions. It has a high internal transmittance in the UV region from 230 to 330 nm, while it is completely opaque in the visible region.

The lamp discharge time, t, should of course be as short as possible. Since $t=(LC)^{0.5}$, where L and C is the inductance and capacitance in the discharge circuit, care should be taken to keep these values low, especially L (C is the energy storage capacitor).

A longer arc length of the lamp, δ, gives a higher conversion efficiency. According to Ref. [7], the maximum conversion also appears at higher discharge energies for longer arc lengths. It also increases the divergence of the outgoing beam, though (cf. eq. 4.6).

A high collection efficiency of the reflector is important for night time measurements, when only the detected pulse energy is of interest. The reflector should thus be a parabola with a MgF_2 protected aluminum coating, or possibly rhodium coated. The aluminum coating reflectance is higher than the rhodium one and is to prefer in the 200-300 nm region. The focal length of the reflector should be large to minimize output beam divergence, which is an important parameter for measurements in daylight .

During daytime measurements these points can be concluded in a formula for the minimum input electrical pulse energy required to obtain an acceptable signal-to-noise ratio by extrapolating from the results here, E_{min}:

$$E_{min,day} \sim \frac{\left[\frac{x_t \delta}{f}\right] * t^{1/2}}{\eta * \Omega} \qquad (8.1)$$

where x_t is the target distance, δ the discharge arc length, f the reflector focal length, t the pulse length, η the lamp conversion efficiency and Ω the reflector collection efficiency. With the lamp and reflector used in the experiments here, having an arc length of 1.5 mm, a reflector focal length of 100 cm, a pulse length of 20 µs, a lamp efficiency of about 3 % and a reflector collection efficiency of about 0.5 %, a discharge energy of about 4000 J would be required to detect the fluorescence light of the weakest fluorescing oil (the Heavy fuel oil E510) in its weakest band (430 nm), at 100 m distance with the detection system described above. The influence of the UV transmitting filter and the reflector has to be taken into account as well. The relation (8.1) is based on the use of a 2 mm thick Schott UG 11 filter and an aluminum coated reflector protected with SiO_2. With this discharge energy, the system will also be able to detect the worst-case oil fluorescence during night time at 300 m distance. The huge electrical discharge energy of 4 kJ per pulse of course is not realistic. Instead the other parameters must be improved. A large factor can be gained by increasing the reflector collection efficiency, still having a long focal length compared to the arc length. The pulse length can be shortened and the lamp conversion efficiency increased. Despite this, however, it seems difficult to find an operative combination that fulfills the requirements. For example, a system employing an EG&G 1PU-1 lamp (Table 4.1) having an arc length of 1 mm and a pulse time of 2µs, and a parabolic reflector with high collection efficiency, the Pichel P9-2 (Table 4.1), still would require about 35 J of discharge energy, which is impossible since the lamp explosion energy is 30 J. Possibly more optimal lamp filters can be found and an even larger reflector can be used. Our conclusion is though, that an airborne flashlamp system for remote characterization of oil slicks will operate close to the detection limit during daytime measurements, no matter what components are chosen for the transmitting system.

For nighttime use, the inference is the opposite, however. Since no background is present, the entire energy output of the lamp can be utilized. A formula for the required lamp energy in this case is to a first order approximation:

$$E_{min,night} \sim \frac{r^2}{\Phi^2 * \Omega * \eta} \qquad (8.2)$$

where r is the target distance, Φ the detection telescope diameter, Ω the reflector collection efficiency and η the lamp conversion efficiency. In our measurements we obtained a good S/N-ratio at r=70 m with E=10 J, Φ=25 cm, Ω=0.005 and η=3%. A small parabolic mirror with a high collection efficiency and a lamp with a somewhat longer arc length yielding a higher conversion efficiency would give a small powerful system, possible to run at a few Hz repetition rate. The divergence of the transmitted beam must not be so large that the image of the illuminated spot partly ends up outside the telescope outcoupling mirror. A flashlamp based system, we infer, thus would constitute an interesting alternative for an airborne oil slick characterizing system for nighttime operation.

ACKNOWLEGEMENTS

Valuable discussions with Olle Fästh, Swedish Space Corporation, are gratefully acknowledged. Discussions with members of the lidar group at our Department have been very fruitful. Special thanks are due to A. Sunesson for making a ramped PMT available to us.

This work was supported by the Swedish Space Corporation.

REFERENCES

1. P. S. Andersson, S. Montán and S. Svanberg, "Oil Slick Characterization Using an Airborne Laser Fluorosensor - Construction Considerations", Lund Reports on Atomic Physics, LRAP-45 (1985).

2. L. Celander, K. Fredriksson, B. Galle and S. Svanberg, "Investigations of Laser-Induced Fluorescence with Applications to Remote Sensing of Environmental Parameters", Göteborg Institute of Physics Reports, GIPR-149 (1978).

3. B. Galle, "Investigation of the Possibility of Detecting Bulk-Transported Chemicals Using Remote Sensing, Based on Laser-Induced Fluorescence", Göteborg Institute of Physics Reports, GIPR-220 (1980) (In Swedish).

4. P. Herder, T. Olsson, E. Sjöholm and S. Svanberg, "Monitoring of Surface Layers Using Fluorescence Techniques", Lund Reports on Atomic Physics, LRAP-9 (1981).

5. An Introduction to Flashlamps, Tecnical Bulletin 1, ILC Technology, 399 Java Drive, Sunnyvale, CA 94089, U.S.A.

6. A Guide to Flashlamps for Solid State Lasers, Technical Bulletin 2, ILC Technology, 399 Java Drive, Sunnyvale, CA 94089, U.S.A.

7. Flashlamps Applications Manual, EG & G Electro-Optics, 355 Congress Street, Salem, Mass. 01970, U.S.A.

8. Optics Guide 3, Melles Griot, 1770 Ketting Street, Irvine, CA 92714, U.S.A.

9. D. M. Hercules (ed.),"Fluorescence and Phosphorescence Analysis", (Wiley, New York 1966).

10. S. Montán, K. Svanberg and S. Svanberg, "Multicolor imaging and contrast enhancement in cancer-tumor localization using laser-induced fluorescence in hematoporphyrin-derivative-bearing tissue", Opt. Lett. 2, 56 (1985).

11. R. Loudon, "The Quantum Theory of Light", Clarendon press, Oxford (1973).